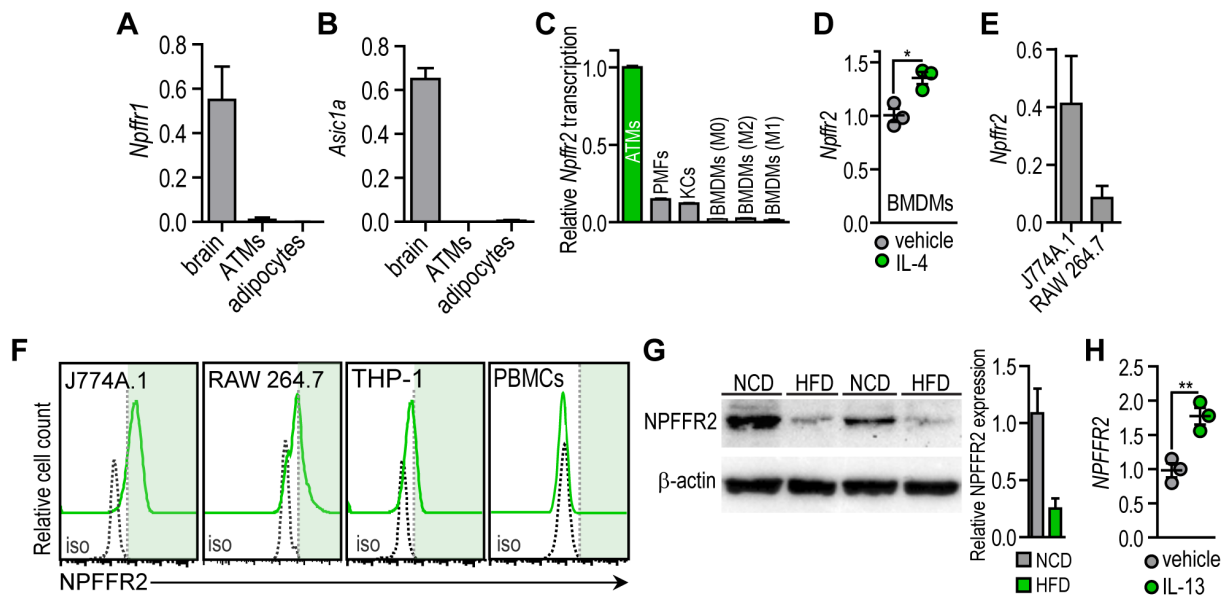


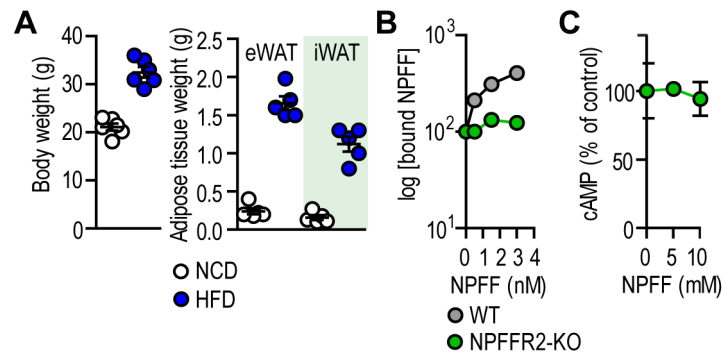
Supplemental Figure 1. Quality control of ATM analysis

(A) FACS analysis of human ATMs from omental fat. (B) Transcript level of *Emr1* (encoding F4/80 antigen) in SVF of eWAT and iWAT from male C57/BL6 mice. (C) ATM content in eWAT and iWAT of lean mice, n=6. (D) FACS analysis of ATMs and immature myeloid cells (iMCs) isolated from lean mouse eWAT and iWAT. The bottom panel shows ATMs after 24 h *in vitro* culture. Further details of ATM characterization have been described previously (1). (E) Relative mRNA transcription of macrophage marker genes in ATM and adipocyte fractions of lean eWAT. We pooled samples from 3–5 male C57/BL6 mice (F) Mouse ATMs were cultured *in vitro* for 24 h. Fluorescent latex beads were added for 1 h to measure phagocytosis activity. Scale bar: 150 μ m. (G) TEM image of a mouse ATM. lp: lamellipodia, nc: nucleus, ph: phagosome. Scale bar: 5 μ m. (H) ATMs cultured *in vitro* for 24 h. Phase contrast image and immunostaining for Mac-3/Lamp-2. Scale bar: 15 μ m. (I) Immunostaining of ATMs for Mac-3/Lamp-2 in the eWAT. Laminin immunostaining was used to mark cell borders. ac: adipocyte, arrows show ATMs. Scale bar: 25 μ m.



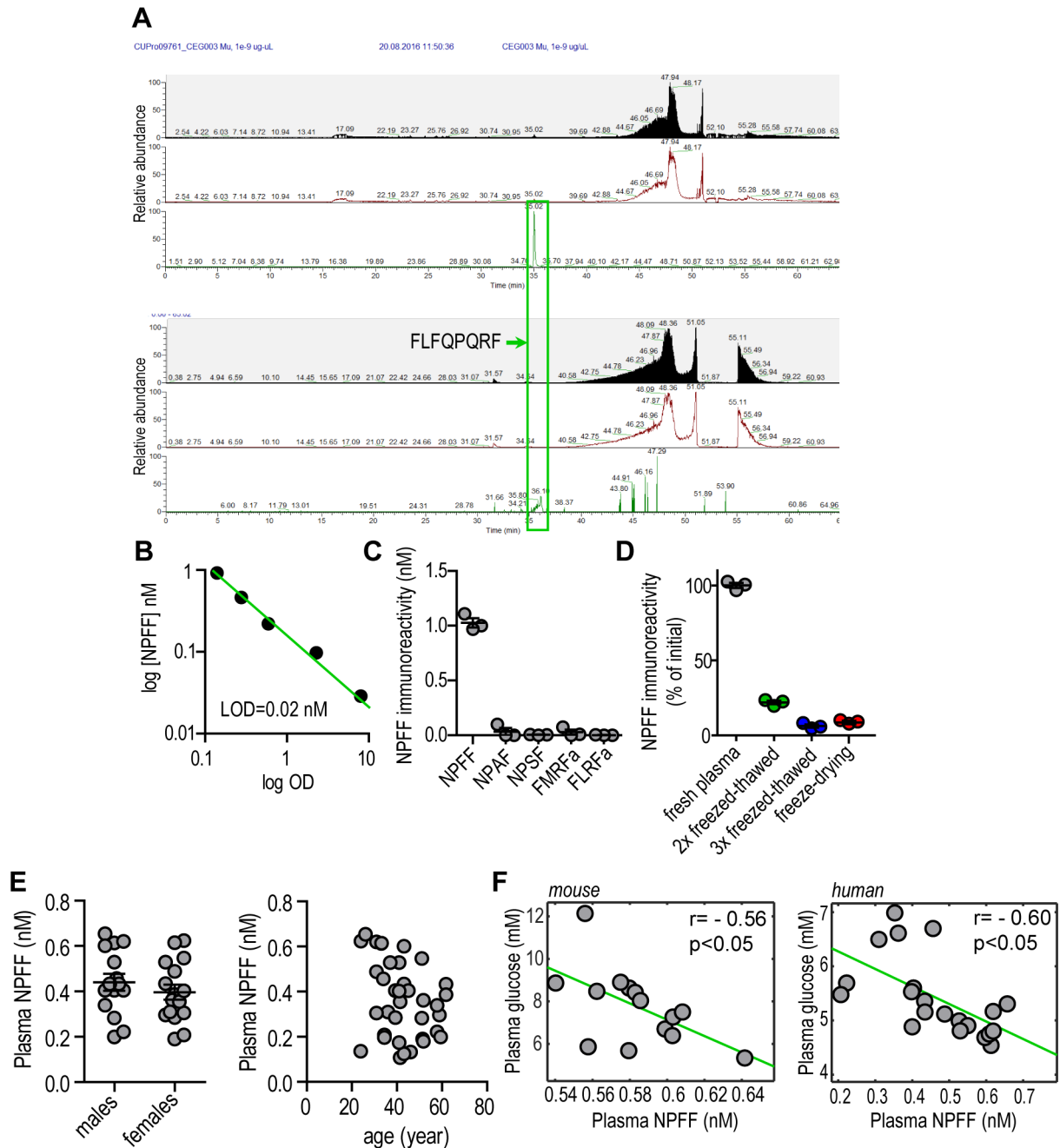
Supplemental Figure 2. Expression of NPFF receptors in macrophages

(A,B) Transcript levels of *Npffr1* and *Asic1a* were measured in ATMs and adipocytes pooled from eWAT and iWAT of 6 mice. Both *Npffr1* and *Asic1a* are known to be expressed by neurons (2-4), thus we used cDNA from brain as a positive control. Transcript levels were normalized to *Bactin* and *Gapdh*, $n=3$. (C) Comparison of *Npffr2* transcript level in various macrophage types in mouse. ATMs: adipose tissue macrophages, PMFs: resident peritoneal macrophages, KCs: Kupffer cells, BMDMs (M0): non-activated bone marrow derived macrophages, BMDMs (M2): BMDMs following 4 h treatment with 10 ng/ml IL-4, BMDMs (M1): BMDMs following 18 h treatment with 100 ng/ml LPS. Transcript level of *Npffr2* in ATMs was set as 1.0, $n=3$. (D) *Npffr2* transcription in non-activated (vehicle-treated) BMDMs and BMDMs treated with 10 ng/ml IL-4 for 4 h. The data set is also shown in panel B, $n=3$. (E) Transcript level of *Npffr2* normalized to *Bactin* and *Gapdh* in mouse macrophage cell lines J774A.1 and RAW 264.7, $n=3$. (F) FACS analysis of NPFFR2 protein expression in J774A.1 and RAW 264.7 cell lines, human monocytic (non-adherent) THP-1 cells and freshly isolated human peripheral blood monocytes (PBMCs). Neither THP-1 cells nor PBMCs were differentiated into macrophages. iso: isotype control. (G) Western blot showing NPFFR2 expression in ATMs isolated after 3 months normal chow diet (NCD) and high-fat diet (HFD) feeding (Left). Pooled ATMs from 6-6 mice. Quantification of western blots showing relative NPFFR2 level, normalized to β -actin as loading control (Right). (H) Effect of 20 ng/ml IL-13 on NPFFR2 transcription in human ATMs. ATMs of the same donor were treated in vitro for 24 h with vehicle or 20 ng/ml IL-13, in triplicate. * $p<0.05$, ** $p<0.01$, Student's unpaired, 2-tailed t-test.



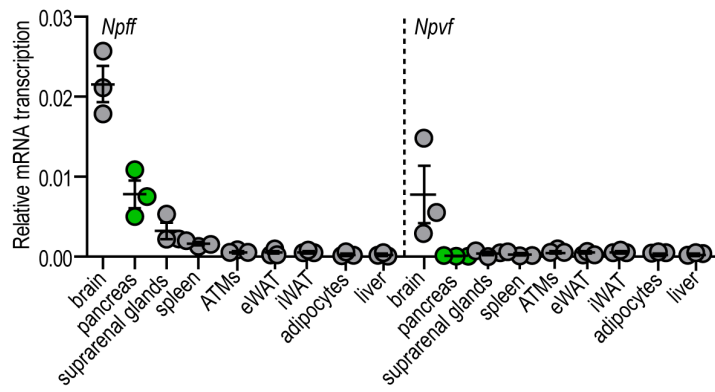
Supplemental Figure 3. Body weight and adipose tissue weight of HFD-fed mice. Lack of NPFF binding by NPFFR2-KO ATMs.

(A) Body weight, and eWAT and iWAT weight of mice on normal chow diet fed (NCD) or high-fat diet (HFD) used in the assay in Figure 1M,N, Figure 2C and Supplemental Figure 2G. (B) NPFF binding by WAT and NPFFR2-KO ATMs using the same assay as in Figure 2A, n=3. Further confirmation of the lack of NPFFR2 activation in NPFFR2-KO cells is shown in Supplemental Figure 13A. (C) Level of intracellular cAMP in NPFFR2-KO macrophages treated with NPFF, using the same assay as in Figure 2B, n=3.



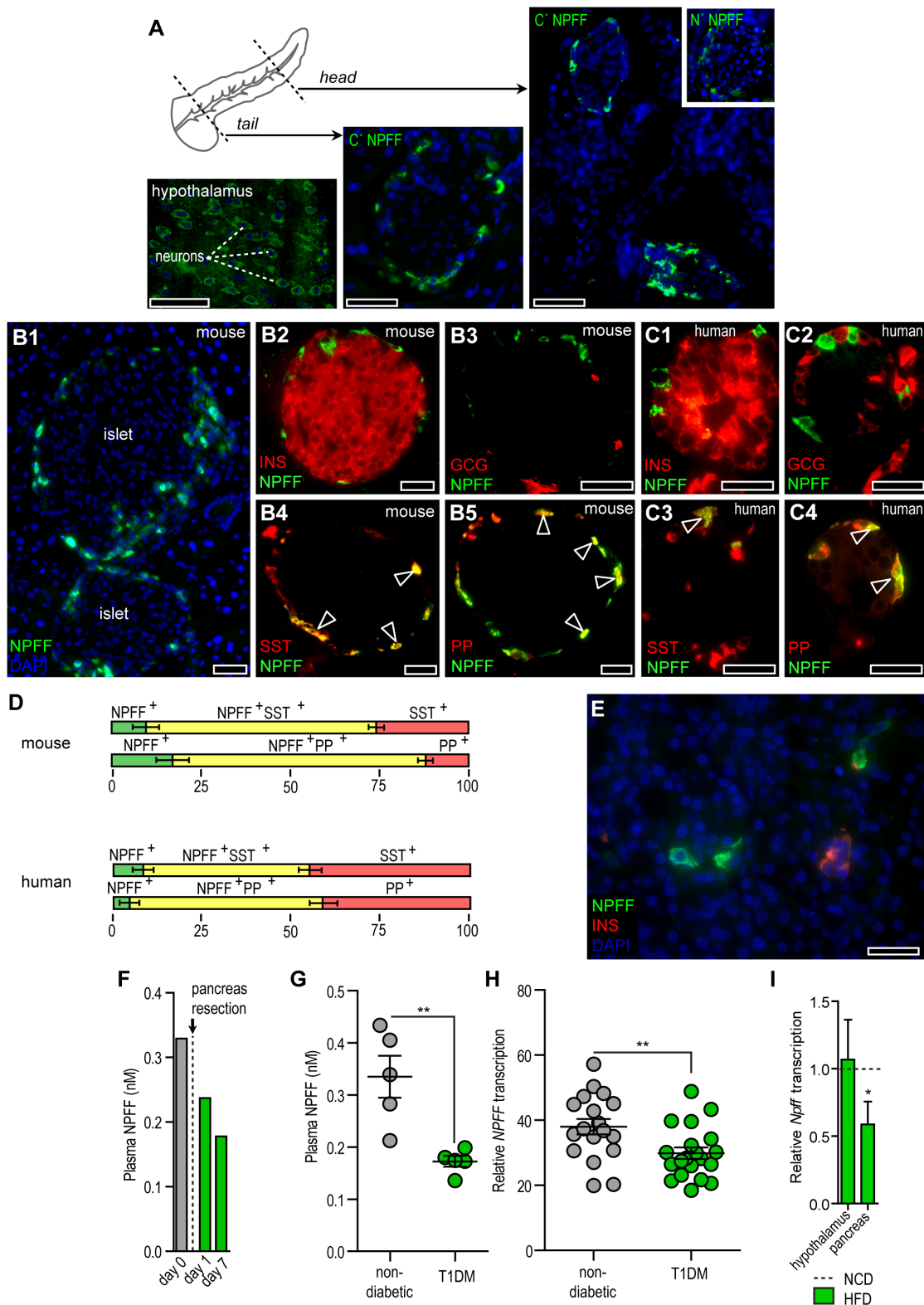
Supplemental Figure 4. Quality control of the NPFF ELISA assay. Age and gender of human subjects enrolled in the study. Correlation between plasma glucose and NPFF level.

(A) Mass spectrometry analysis of plasma. *Top*: NPFF standard added to native human plasma, *Bottom*: NPFF peak in native human plasma (0.36 nM, obese blood donor). (B) Representative calibration curve of the ELISA assay using synthetic NPFF as standard. (C) Specificity of the ELISA assay was controlled using 1 nM of various RF-amides. (D) Effect of freeze-thaw cycles on the NPFF content of human plasma. Three samples were assayed immediately after obtaining blood; following two or three freeze-thaw cycles or freeze-drying. Initial NPFF level was set at 100%. (E) Plasma NPFF in males and females enrolled in the study (*Left*). Plasma level and age of healthy volunteers and morbidly obese patients enrolled in the study (*Right*). (F) Correlation matrix of plasma glucose and NPFF levels in mouse and in human. Two-way ANOVA.



Supplemental Figure 5. Expression of *Npff* in peripheral tissues

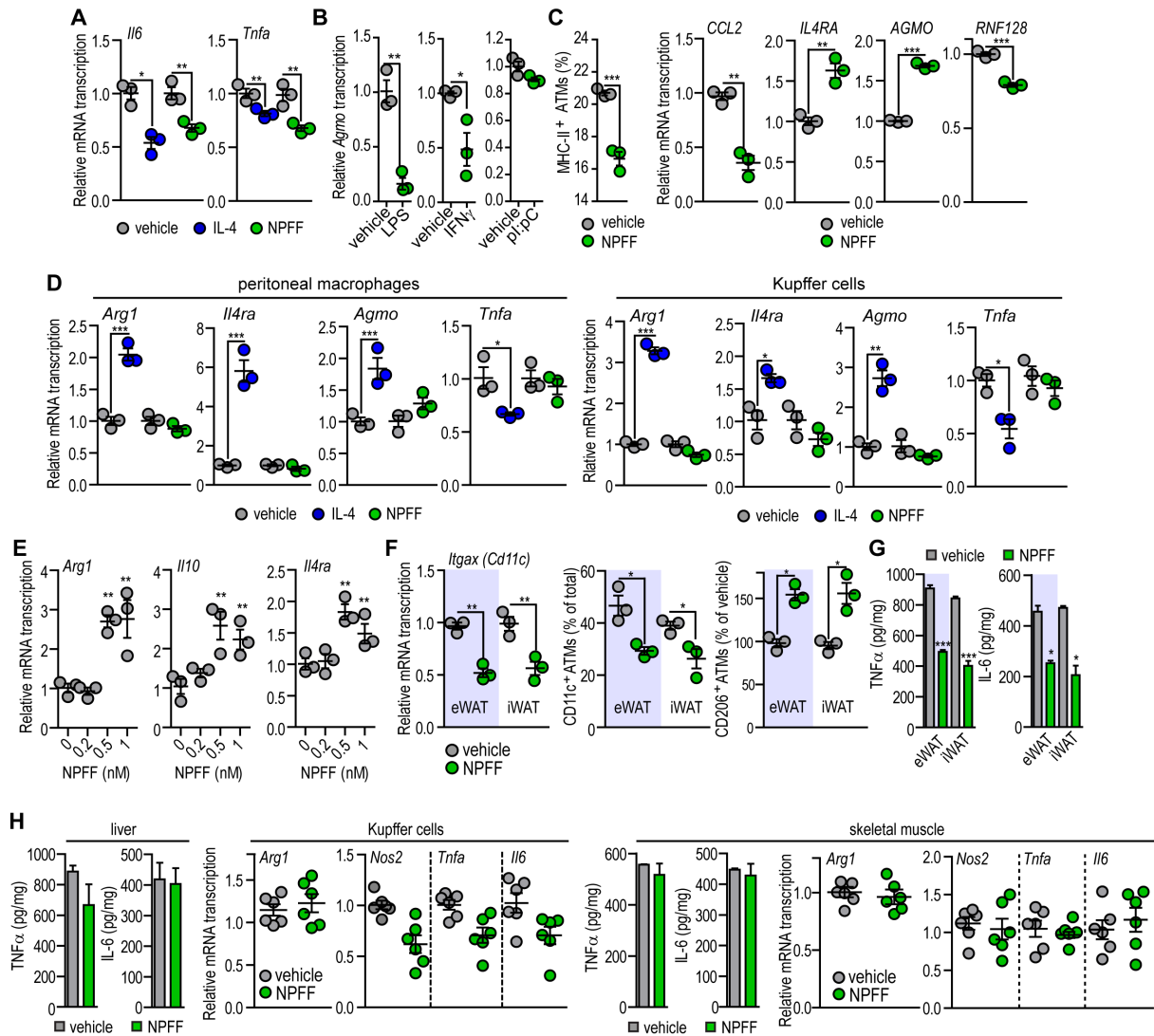
Npff and *Npvf* transcription in mouse organs and cells (n=3). *Npvf* encodes an RF-amide that is structurally related to NPF (4). Values are normalized to *Bactin*. Pancreas had notable *Npff* transcription, which was analyzed in more detail (see Supplemental Figure 6).



Supplemental Figure 6. Distribution of NPFF in mouse and human pancreatic islets

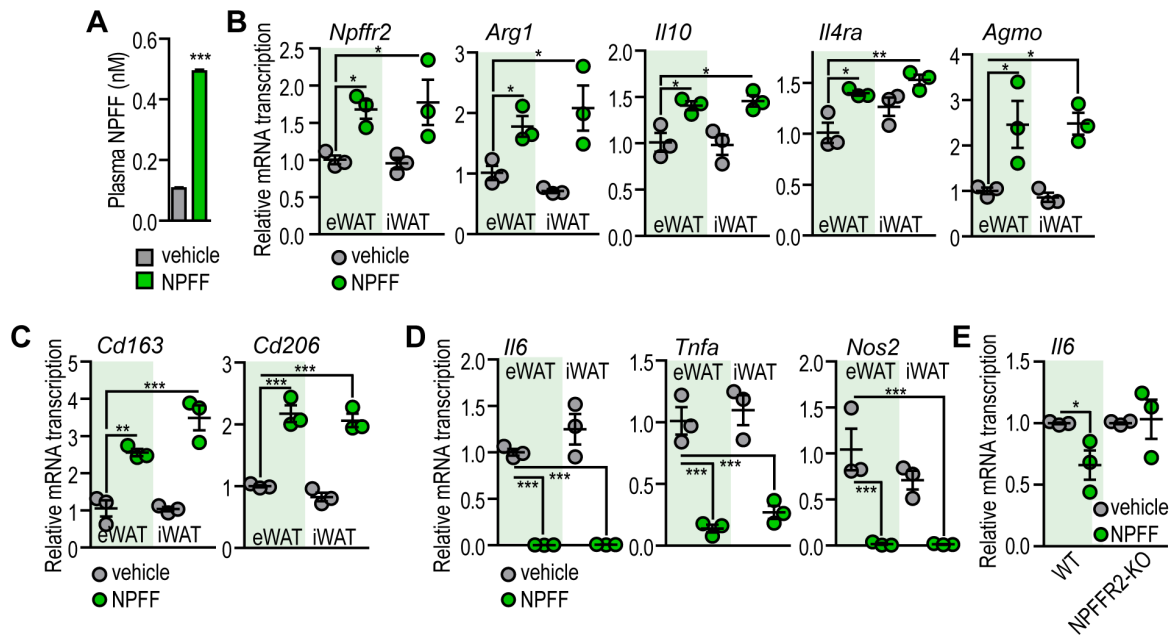
(A) Schematic diagram showing the regions of histological analysis with representative images from the respective pancreas regions. C' NPFF: staining with an antibody raised against the C-terminus of NPFF. N' NPFF: staining with an antibody raised against the N-terminus of NPFF. Mouse hypothalamus was used as a positive control. Scale bar: 100 μ m. (B,C) Distribution of NPFF in mouse pancreatic islets (B1–B5) and in human pancreatic islets (C1–C4). INS: insulin, GCG: glucagon, SST: somatostatin, PP: pancreatic polypeptide. Scale bars: 100 μ m (B1) and 25 μ m (B2–C4). Arrowheads indicate co-localization of NPFF with SST and PP. (D) Percentage of NPFF-expressing endocrine cells in mouse and human pancreatic islets. (E) NPFF and insulin (INS) staining of non-islet-associated endocrine cells in human pancreas. Scale bar: 50 μ m. (F) Plasma NPFF

levels in a patient who underwent radical pancreas resection. NPF levels were assayed before surgery (day 0) and after removal of the pancreas (day 1, day 7). Within this time window the patient did not receive a blood transfusion. The reduction in plasma NPF levels after pancreas resection suggests that pancreas releases NPF into the bloodstream. **(G)** NPF was expressed by non-beta cells of the islets, and in type 1 diabetic patients (T1DM) the non-beta cells can convert into beta cells (5). We hypothesize that this may cause the loss of *NPF* transcription. Accordingly, in our cohort we observed strong reduction of plasma NPF level in T1DM patients. **(H)** Consistent with the reduced plasma NPF levels, relative transcription of *NPF* was reduced in pancreatic islets of T1DM patients. Each data point represents Affymetrix analysis of one patient. Islets were collected with laser capture microdissection. **(I)** Relative transcription of pancreatic and hypothalamic *Npff* in HFD-fed mice; dotted line indicates transcript level in NCD-fed mice, n=6. Student's unpaired, 2-tailed t-test, *p<0.05, **p<0.01.



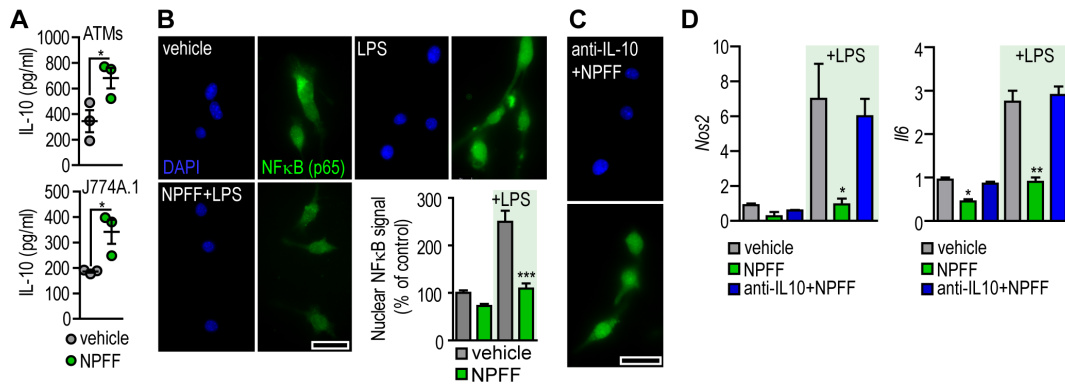
Supplemental Figure 7. Effect of NPFF on macrophage activation

(A) Relative transcription of M1 genes *Il6* and *Tnfa* in ATMs treated with 10 ng/ml IL-4 or 0.5 nM NPFF for 4 h, n=3. (B) Relative transcription of *Agmo* in J774A.1 macrophages in response to LPS and interferon signaling. Applied treatments: 100 ng/ml LPS for 18 h, 2.5 ng/ml IFN γ for 4 h, 5 μ g/ml pI:pC for 4 h. (C) Percentage of MHC-II⁺ human ATMs treated in vitro with vehicle or 0.5 nM NPFF for 18 h, n=3. Transcription of *CCL2*, *IL4RA*, *AGMO* and *RNF128* in human ATMs treated in vitro with vehicle or 0.5 nM NPFF for 4 h, n=3. (D) Transcript level of *Arg1*, *Il4ra*, *Agmo* and *Tnfa* in peritoneal macrophages and Kupffer cells treated in vitro with vehicle, 10 ng/ml IL-4 for 4 h, or 0.5 nM NPFF for 4 h, n=3. (E) Dose-response of NPFF in ATMs. Mouse ATMs were treated for 1 h with vehicle, 0.2, 0.5 or 1 nM NPFF, and the transcription of *Arg1*, *Il10* and *Il4ra* was measured. Each data point represents pooled ATMs from 3-5 mice. (F) Transcription of *Itgax (Cd11c)* in mouse ATMs, and frequency of CD206⁺ and CD11c⁺ ATMs after in vivo treatment with vehicle or NPFF (Treatment scheme is shown in Figure 2H). Each data point represents pooled ATMs from 2-2 mice. (G) Level of TNF α and IL-6 in eWAT and iWAT of HFD-fed mice, treated with vehicle or NPFF (Treatment scheme is shown in Figure 2H). (H) Level of TNF α and IL-6 in liver and quadriceps muscle, and transcription of *Arg1*, *Nos2*, *Tnfa* and *Il6* in Kupffer cells and quadriceps muscle following vehicle or NPFF treatment in vivo, n=6. Treatment scheme is shown in Figure 2H. Student's unpaired, 2-tailed t-test (A,B,C,F,G,H) and one-way ANOVA with Dunnett's post-hoc test (D,E), *p<0.05, **p<0.01, ***p<0.001.



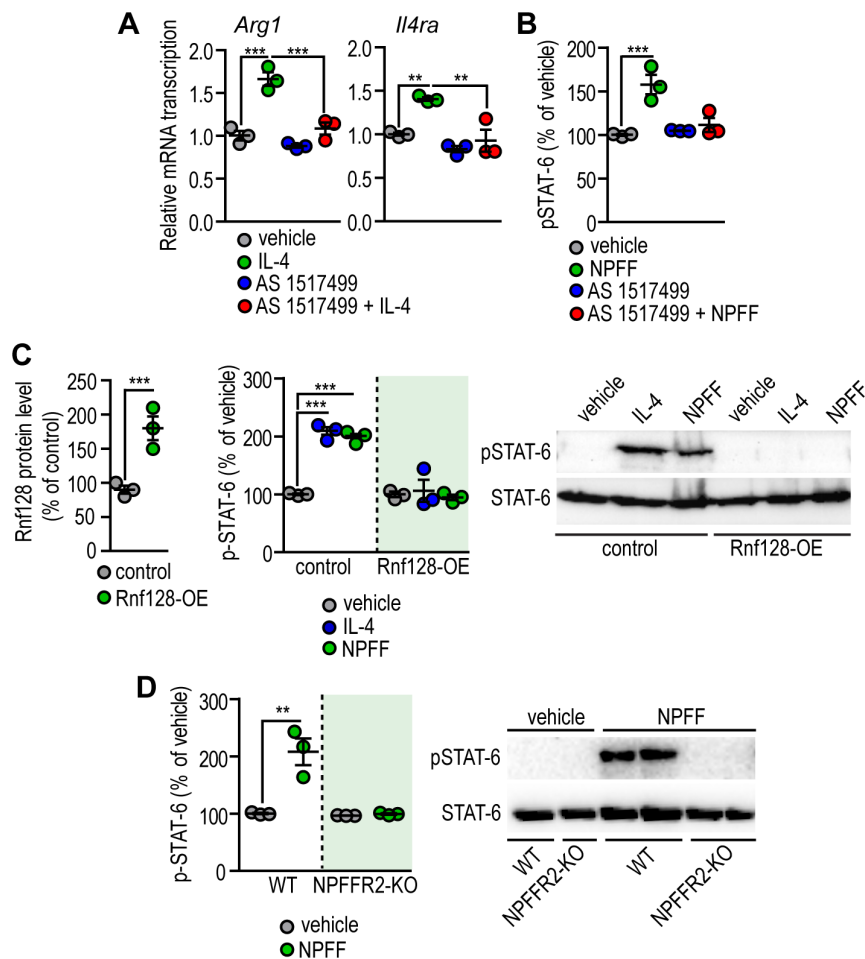
Supplemental Figure 8. Plasma level of NPFF in HFD-fed mice after 18 days of NPFF replacement. Effect of NPFF replacement on ATM activation in HFD-fed mice.

(A) Plasma level of NPFF in vehicle-treated or NPFF-treated mice. Treatment scheme is shown in Figure 2H. Metabolic parameters are summarized in Figure 3. (B–D) Transcript level of *Npffr2*, M2 and M1 activation genes in ATMs following NPFF treatment. Treatment scheme is shown in Figure 2H. The data set shown here matches the analysis shown in Figure I–K, but using eWAT vehicle for normalization. This representation allows the comparison of transcript levels between eWAT and iWAT. It has been shown that visceral and subcutaneous fat depots can develop comparable inflammatory state in obesity (6, 7). (E) Transcript level of *Il6* in wild-type (WT) and NPFFR2-KO ATMs, treated with 0.5 nM NPFF for 4 h, n=3. Student's unpaired, 2-tailed t-test (A,E) and one-way ANOVA with Dunnett's post-hoc test (B–D).



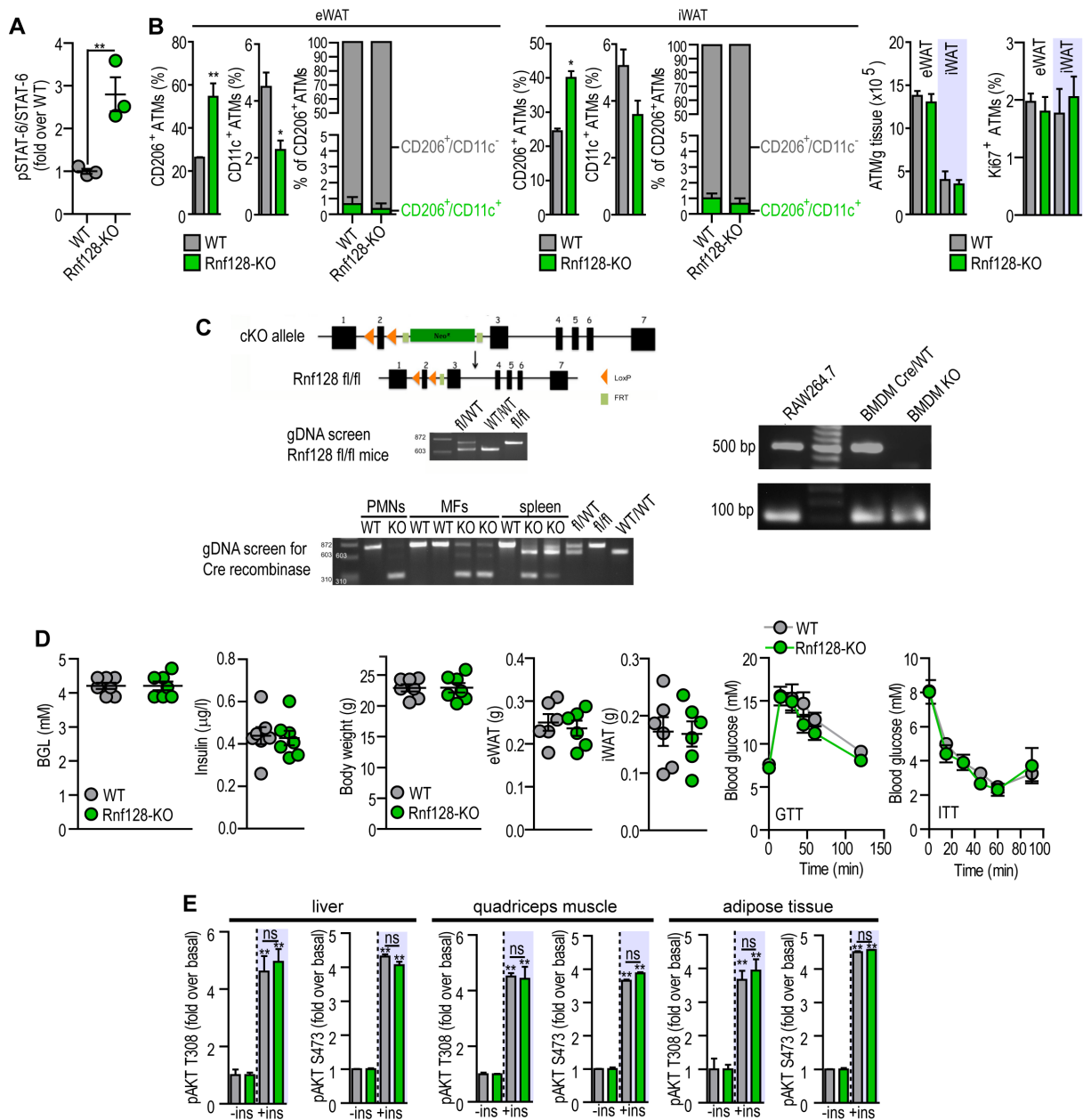
Supplemental Figure 9. Effect of NPFF on macrophage activation

(A) IL-10 secretion by ATMs and J774A.1 cells treated with 0.5 nM NPFF for 4 h, measured in culture medium by ELISA, n=3. (B) Nuclear translocation of NFκB in response to 100 ng/ml LPS and 1 nM NPFF. Cells were treated for 40 minutes. Scale bar: 50 μm. (C) Nuclear translocation of NFκB in response to LPS and NPFF in the presence of IL-10 neutralizing antibody (1:500 dilution, raised in rabbit). Scale bar: 50 μm, n=6. (D) Effect of 100 ng/ml LPS, 0.5 nM NPFF and IL-10 neutralizing antibody on M1 activation of ATMs. Mouse ATMs were cultured *in vitro*, treated with vehicle, 0.5 nM NPFF, 100 ng/ml LPS or their combination for 6 h. Transcript level of *Nos2* and *Il6* was measured. The effect of NPFF on transcriptional changes was tested also in the presence of IL-10 neutralizing antibody (1:500 dilution, raised in rabbit), n=3, using ATMs pooled from 3 mice. *p<0.01, **p<0.05, ***p<0.001, Student's unpaired, 2-tailed t-test.



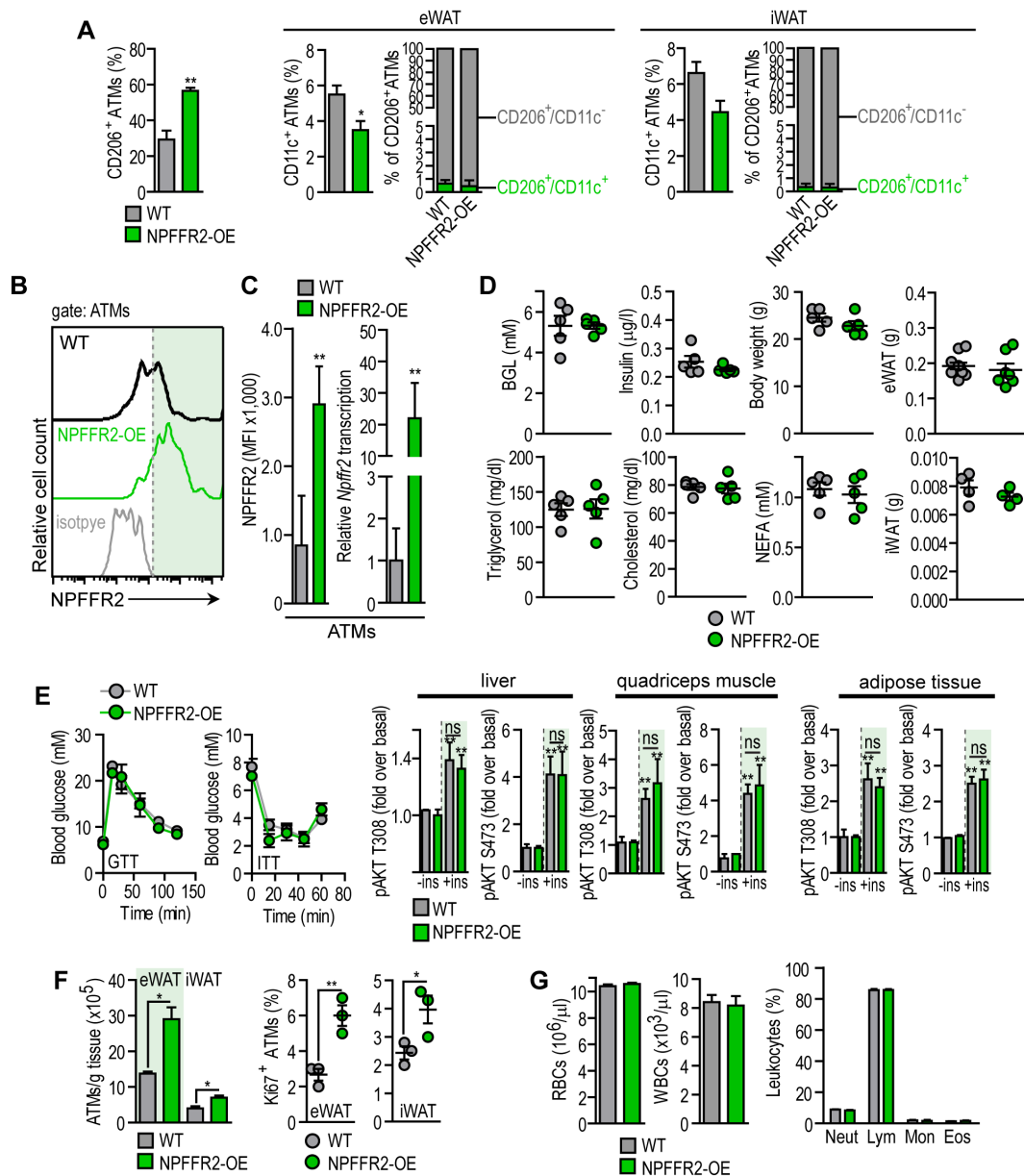
Supplemental Figure 10. NPFF signaling through STAT-6 in macrophages

(A) Relative transcription of the STAT-6 target genes *Arg1* and *Il4ra* in ATMs treated with vehicle, STAT-6 inhibitor AS 1517499 (200 nM), 10 ng/ml IL-4 or their combination for 1 h, n=3. (B) Relative level of pSTAT-6 (normalized to STAT-6) in ATMs treated with 0.5 nM NPFF, STAT-6 inhibitor AS 1517499 (200 nM) or their combination for 30 min, measured by in-cell ELISA, n=3. (C) Protein level of Rnf128 in control and Rnf128-overexpressing (Rnf128-OE) J774.A1 macrophages (Left). Relative level of pSTAT-6 (normalized to STAT-6) in control and Rnf128-OE J774.A1 macrophages following 0.5 h treatment with vehicle, IL-4 (10 ng/ml) or NPFF (0.5 nM), n=3 (Middle). Western blot of pSTAT-6 and STAT-6 in control and Rnf128-OE J774.A1 macrophages following 0.5 h treatment with vehicle, IL-4 (10 ng/ml) or NPFF (0.5 nM) (Right). Representative blot from two independent experiments. (D) Relative level of pSTAT-6 in ATMs of WT and NPFFR2-KO mice following 0.5 h treatment with vehicle or 0.5 nM NPFF, measured by in-cell ELISA, n=3. Representative western blot of pSTAT-6 and STAT-6 in ATMs of WT and NPFFR2-KO mice following 0.5 h treatment with vehicle or 0.5 nM NPFF (from two independent assays). One-way ANOVA with Dunnett's post-hoc test (A,B,C Middle, D), and Student's unpaired, 2-tailed t-test (C Left), **p<0.01, ***p<0.001.



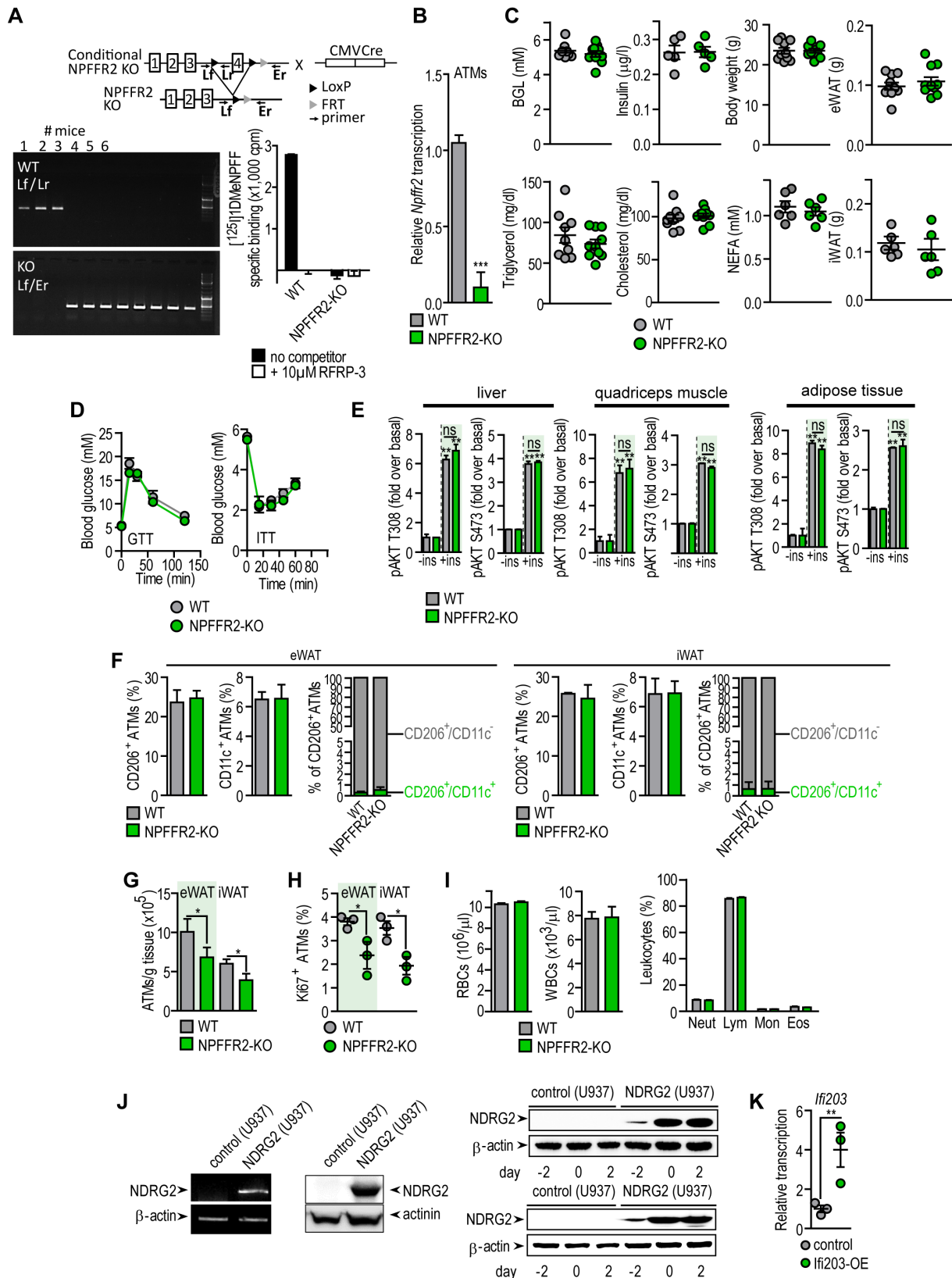
Supplemental Figure 11. Transgenic mice and cells used in this study: Rnf128-KO mouse

(A) Level of pSTAT-6 normalized to total STAT-6 in wild-type (WT) and Rnf128 deficient (Rnf128-KO) ATMs, n=3. (B) Amount of CD206⁺, CD206⁺/CD11c⁻ (M2 activated (8, 9)) and CD11c⁺, CD206⁺/CD11c⁺ (pro-inflammatory (8-10)) ATMs in WT and Rnf128-KO mice. Number of ATMs, and percentage of Ki67⁺ ATMs in adipose tissue depots of WT and Rnf128-KO mice, n=3. (C) Scheme of germline Rnf128 targeting vector (*Top*) and PCR of genomic DNA from WT and KO mice. PMNs: peritoneal macrophages, MFs: bone marrow-derived macrophages. Rnf128 expression in WT and KO bone marrow-derived macrophages (BMDMs). (D) Metabolic phenotype of WT and Rnf128-KO mice: body weight, basal glucose level (BGL) and insulin level, GTT, ITT, adipose tissue weight, n=7. (E) Insulin-induced phosphorylation of AKT in liver, quadriceps muscle and adipose tissue (eWAT). Level of phosphorylated AKT (pAKT) T308 and pAKT S473 was measured by ELISA and normalized to total AKT. -ins: without insulin, +ins: 15 min following insulin stimulation, n=3, one-way ANOVA with Dunnett's post-hoc test, *p<0.05, **p<0.01. Student's unpaired, 2-tailed t-test (A,B), *p<0.05, **p<0.01, ns: non-significant.



Supplemental Figure 12. Transgenic mice and cells used in this study: NPFFR2-OE mouse

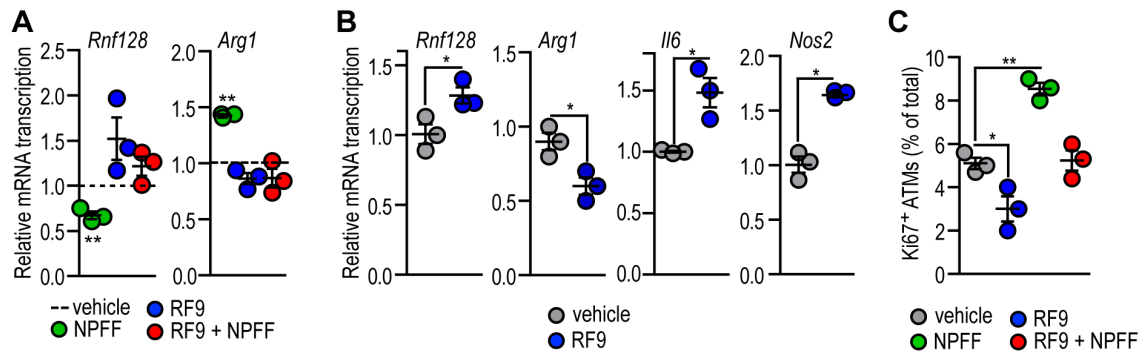
(A) Amount of CD206⁺ ATMs in iWAT (corresponding data for eWAT are shown in Figure 4J), and CD11c⁺, CD206⁺/CD11c⁻ and CD206⁺/CD11c⁺ ATMs in WT and NPFFR2-OE mice, n=6. (B) FACS analysis of NPFFR2 in ATMs of WT and NPFFR2-OE mice, n=3. (C) Expression of NPFFR2 protein and *Npffr2* mRNA in WT and NPFFR2-OE ATMs, n=6. MFI: mean fluorescence intensity (D,E) Metabolic parameters of WT and NPFFR2-OE mice, n=6: BGL, basal insulin level, plasma lipid profile, body weight, adipose tissue weight, GTT, ITT, insulin-induced phosphorylation of AKT. Level of pAKT T308 and pAKT S473 was measured by ELISA. -ins: without insulin, +ins: 15 min following insulin stimulation, n=3, one-way ANOVA with Dunnett's post-hoc test, *p<0.05, **p<0.01. (F) Amount of CD206⁺, CD206⁺/CD11c⁻ and CD206⁺/CD11c⁺ ATMs, n=3. Number of ATMs, and percentage of Ki67⁺ ATMs in adipose tissue depots of WT and NPFFR2-OE mice, n=6. (G) Hematology of WT and NPFFR2-OE mice, n=3. Student's unpaired, 2-tailed t-test (A,C,F), *p<0.05, **p<0.01.



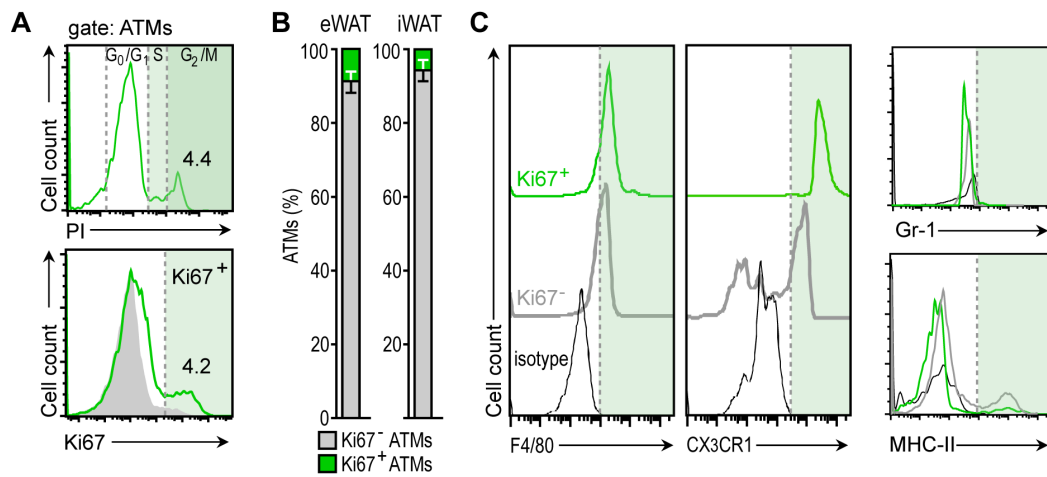
Supplemental Figure 13. Transgenic mice and cells used in this study: NPFFR2-KO mouse, NDRG2-overexpressing and Ifi203-overexpressing macrophages

(A) Schematic illustration of NPFFR2 knockout (KO) mouse generation and characterization. Conditional NPFFR2-KO vector contains exon 4 flanked by LoxP sequences (black triangles), and FRT sequences (gray triangles). Conditional NPFFR2-KO mice were crossed with Cre-CMV mice to generate NPFFR2-KO mice. PCR primers are represented by black arrows. Neomycin resistance cassette deletion using FRT sequences is not shown. Results of genotyping PCR of 6 littermate mice (#1-6), using genomic DNA (*lower left panel*). The image shows genotyping PCR of further five NPFFR2-KO mice. Olfactory bulb homogenates from NPFFR2-

KO animals displayed no [¹²⁵I]1DMeNPFF binding sites compared with WT animals, showing the absence of NPFFR2 in these animals (*lower right panel*). Cold RFRP3 that binds with affinity to both NPFFR1 and NPFFR2 fully blocked [¹²⁵I]1DMeNPFF binding in WT animals indicating that it is specifically due to NPFF receptors. **(B)** Relative mRNA level of *Npffr2* in WT and NPFFR2-KO ATMs, n=6. **(C,D)** Metabolic parameters of WT and NPFFR2-KO mice, n=7–11. NEFA: non-esterified fatty acids **(E)** Insulin-induced phosphorylation of AKT. Level of pAKT T308 and pAKT S473 was measured by ELISA and normalized to total AKT. –ins: without insulin, +ins: 15 min following insulin stimulation, n=3, one-way ANOVA with Dunnett's post-hoc test, *p<0.05, **p<0.01. **(F)** Amount of CD206⁺, CD11c⁺, CD206⁺/CD11c⁻ and CD206⁺/CD11c⁺ ATMs in WT and NPFFR2-KO mice, n=3. **(G)** Number of ATMs and **(H)** percentage of Ki67⁺ ATMs in adipose tissue depots of WT and NPFFR2-KO mice, n=6. **(I)** Hematology of WT and NPFFR2-KO mice, n=6. **(J)** Expression of NDRG2 in control and NDRG2-OE U937 macrophages. **(K)** Relative transcription of *Ifi203* in control and Ifi203-OE J774A.1 macrophages. Student's unpaired, 2-tailed t-test (B,G), *p<0.05, ***p<0.001.

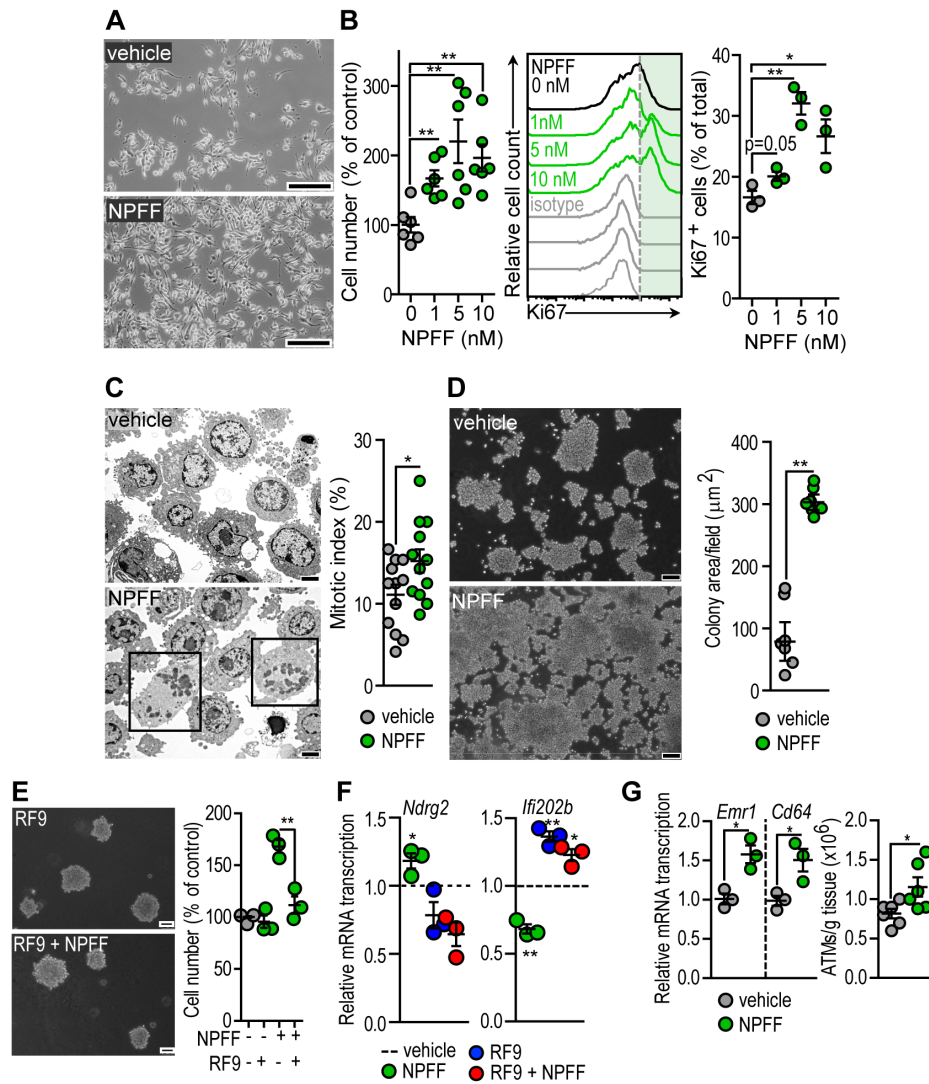


Supplemental Figure 14. Effect of pharmacological NPFf receptor inhibition on macrophage activation
(A) Effect of 10 nM RF9 on the transcriptional changes evoked by 0.5 nM NPFF within 0.5 h in J774A.1 macrophages, n=3. **(B)** HFD-fed mice were treated with i.p. injection of RF9 (10 nmol/kg/day) for 7 days. Transcription of *Rnf128*, *Arg1*, *Il6* and *Nos2* was measured in ATMs, n=3. Note the antagonistic effect of RF9 on NPFF. **(C)** Ki67⁺ ATMs following NPFF (4 nmol/kg/day), RF9 treatment (10 nmol/kg/day) or their combination for 7 days in normal chow diet fed mice, n=3. NPFF treatment also increased total ATM number by 21.2±3.2%, when compared to vehicle (p<0.01). *p<0.05, **p<0.01, one-way ANOVA with Dunnett's post-hoc test (A,C), Student's unpaired, 2-tailed t-test (B).



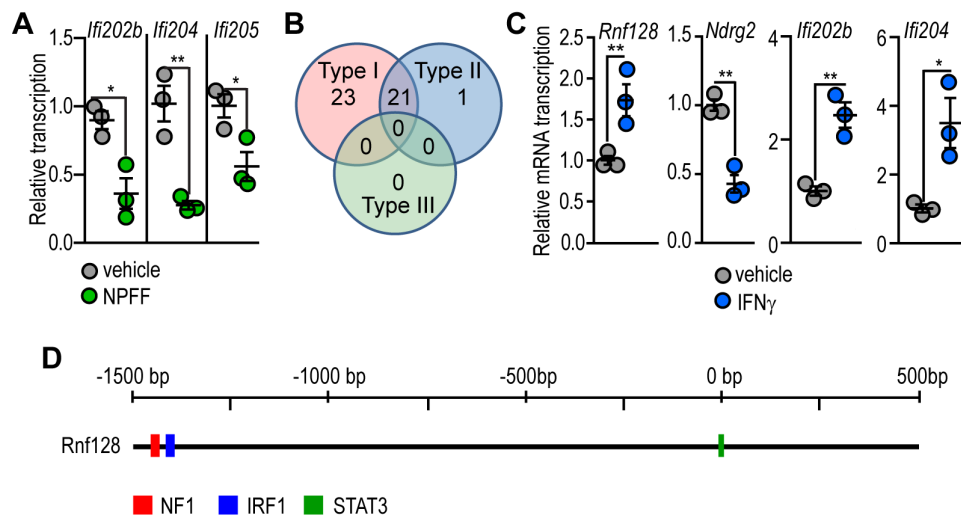
Supplemental Figure 15. Self-renewing ATMs in lean adipose tissue

(A) Histograms showing DNA content (using propidium iodide (PI) staining) and Ki67 antigen expression of ATMs isolated from eWAT of lean C57BL/6 mice, n=6. (B) Ki67⁻ and Ki67⁺ ATM content of eWAT and iWAT in lean mice, n=6. (C) FACS analysis of Ki67⁻ and the Ki67⁺ ATMs in lean mice showing expression of macrophage marker F4/80 antigen, chemokine receptor CX₃CR1, granulocyte marker Gr-1, and MHC-II.



Supplemental Figure 16. Effect of NPFF on J774A.1 macrophage proliferation. ATM count in NPFF-treated mice

(A) Overview of control (vehicle-treated) and NPFF treated (1 nM, 18 h) J774A.1 macrophage cultures. Scale bar: 100 μm . (B) Cell number and quantity of Ki67⁺ cells following 18 h treatment with NPFF in J774A.1 macrophage cultures, n=6. (C) Transmission electron microscopy (TEM) of vehicle- and NPFF-treated macrophages. Scale bar: 0.5 μm . Frames indicate macrophages in mitosis. Mitotic index was determined using TEM images. Each point represents one field. (D) Colonies of J774A.1 macrophages grown for one week in soft agar. Scale bar: 100 μm . NPFF was added at 1 nM, n=7. (E) Colony forming assay and cell count after treatment with 10 nM RF9 or 1 nM NPFF for one week (colony forming assay) or for 18 h (cell count). (F) Effect of RF9 on the transcriptional changes evoked by 0.5 nM NPFF within 0.5 h. (G) Transcription of macrophage marker genes and ATM count in iWAT of vehicle- or NPFF-treated, HFD-fed mice. Treatment scheme is shown in Figure 2H; each data point represents pooled ATMs from 3-3 mice (gene transcription data), and n=6 (ATM number). Student's unpaired, 2-tailed t-test; $p < 0.05$, $**p < 0.01$, $***p < 0.001$.



Supplemental Figure 17. Effect of NPF on interferon-regulated gene expression

(A) Relative transcription of *Ifi202b*, *Ifi204*, *Ifi205* in control and NPF treated (0.5 nM, 0.5 h) J774A.1 macrophages, n=3. (B) Venn diagram of NPF suppressed genes of type 1 and type 2 interferon response (DNA chip results are available under GEO Accession Number GSE90658). (C) Effect of 4 h treatment with 2.5 ng/ml IFN γ on NPF-regulated genes in J774A.1 macrophages, n=3. Student's unpaired t-test, *p<0.05, **p<0.01. (D) Transcription factor binding site analysis of *Rnf128*, using Interferome v2.0 (11).

Supplemental Table 1. List of antibodies used in FACS analysis and immunostaining	
Antigen, conjugate	Commercial source, reference of clone number
human KI67, APC	Affymetrix eBioscience, 20Raj1
human arginase-1, AF488	Affymetrix eBioscience, Sl6arg
human CD68, PECy7	Affymetrix eBioscience, Bio Y1/82A
mouse Ki67, PE Cy7	Affymetrix eBioscience, SolA15
mouse MHC-II, AF700	Affymetrix eBioscience, MS/114.15.2
mouse CD206, FITC	BioLegends, C068C2
mouse Gr-1 (Ly6G), PE or PECy7	Affymetrix eBioscience, RB6-805 or RB6-8C5
mouse CD45, PeCy5.5 or APC	Affymetrix eBioscience, 30-F11 or 30-F11
BrdU, PE	Affymetrix eBioscience, BU20A
mouse CD11b, APC or AF700	Affymetrix eBioscience, M1/70
mouse CD14, PE	BD Pharmingen, mC5-3
mouse Mac-3 (Lamp-2), PE	BD Pharmingen, 553324
mouse F4/80, APC or PE	Affymetrix eBioscience, BM8
mouse TNF α , eFluor 450	Affymetrix eBioscience, MP6-XT22
human/mouse glucagon, unconjugated	R&D Systems, Minneapolis, USA, clone 181402, mono ms IgG2A
human/mouse pancreatic polypeptide, unconjugated	R&D Systems, Minneapolis, USA, ref. no. AF6297, polyclonal goat IgG
human/mouse somatostatin, unconjugated	R&D Systems, Minneapolis, USA, clone 906552, monoclonal rat IgG1
human/mouse insulin, unconjugated	AbCam, Cambridge, UK, guinea pig polyclonal, ref. no. ab7842
human/mouse NPPFR2, unconjugated	Biorbyt LLC, San Francisco, USA; ref. no. orb31952, rabbit polyclonal
NPFF C-terminal, unconjugated	Biorbyt LLC, San Francisco, USA; ref. no. orb35548, rabbit polyclonal
NPFF N-terminal, unconjugated	Cloud Clone Corp., Wuhan, PRC, Ref. no. PAG003Ra08, rabbit polyclonal
human/mouse MAFB, unconjugated	DSHB The University of Iowa, USA; ref.no. PCR-P-MAFB-1A10-s
mouse/human CX ₃ CR1, unconjugated	AbCam, Cambridge, UK, ref. no. ab8021, rabbit polyclonal
NF κ B, unconjugated	Cell Signaling Technology, Danvers, USA, ref. no. 4764, rabbit polyclonal
mouse F4/80, unconjugated	Santa Cruz Biotech, Dallas, TX, USA, sc25830, rabbit polyclonal
mouse laminin, unconjugated	AbCam, Cambridge, UK, ref. no. ab11575, rabbit polyclonal
human NDRG2	Santa Cruz Biotechnology, goat polyclonal
human alpha-actinin	Santa Cruz Biotechnology, mouse monoclonal
mouse β -actin	Cell Signaling Technology, Danvers, USA, ref.no.13E5, rabbit polyclonal
mouse STAT6	Cell Signaling Technology, Danvers, USA, ref.no.9362, rabbit polyclonal
mouse pSTAT6 (Tyr641)	Cell Signaling Technology, Danvers, USA, ref.no. 9361, rabbit polyclonal
secondary antibodies	donkey anti rabbit TRITC, Novex A16040; donkey anti goat AF546 Life Technologies A11056; goat anti rabbit AF594, Life Technologies A11037; goat anti mouse AF488 Life Technologies A11001; goat anti guinea pig AF488 Life Technologies A11073

Supplemental Table 2. Primer sequences used in qPCR analysis	
Mouse genes	Sequence
<i>Rnf128</i>	Fw: TGCTTGTAGGAGCTGCGTCT
	Rev: AGCCAGAAGGAAGCACCAAG
<i>Il4ra</i>	Fw: CACCTGGAGTGAGTGGAGTC
	Rev: AGGCAAAACAACGGGATG
<i>Arg1</i>	Fw: CATTGGCTTGCAGACGTAGAC
	Rev: GCTGAAGGTCTCTTCCATCACC
<i>Agmo</i>	Fw: CTTTCTTAGGAGTTGACTTTGGCTACT
	Rev: TGTGCTGCCAGAAAATATTAATC
<i>Il10</i>	Fw: TCGGAAATGATCCAGTTTAC
	Rev: TCACTCTTCACTGCTCCAC
<i>Ndrp2</i>	Fw: TCCTTTGGCCGCACTAACTT
	Rev: CACGCTCTACACGTCACAGT
<i>Ifi202b</i>	Fw: AAGTCCCAGGCTGCAGAAC
	Rev: TCCAGGAGAGGCTTGAGGTT
<i>Ifi204</i>	Fw: CAGGGAAAATGGAAGTGGTG
	Rev: CAGAGAGGTTCTCCCGACTG
<i>Ifi205</i>	Fw: CAAGCAGGCCACTTCTGTTG
	Rev: TCAAACGGGTCTGTTGCAGT
<i>Ifi 203</i>	Fw: CCCAGGAAGACAGCACACTA
	Rev: CCGCCAGCTGAATCCTATCA
<i>Mafb</i>	Fw: AGGACCGCTTCTCTGATGAC
	Rev: GAGCTGCGTCTTCTCGTTCT
<i>Cycline</i>	Fw: TCAGTGGTGCACATAGAGAA
	Rev: TGTCCAGCAAATCCAAGCTG
<i>Bactin</i>	Fw: GCACCAGGGTGTGATGGTG
	Rev: CCAGATCTTCCATGTCGTCC
<i>Ppia (Cypa)</i>	Fw: ATTTCTTTGACTTGCGGGC
	Rev: AGACTTGAAGGGGAATG
<i>Nos2</i>	Fw: GAGACAGGGAAGTCTGAAGCAC
	Rev: CCAGCAGTAGTTGCTCCTCTTC
<i>Tnfa</i>	Fw: TGCCTATGTCTCAGCCTCTTC
	Rev: GAGGCCATTTGGGAACTTCT
<i>Il6</i>	Fw: GCTACCAAAGTGGATATAATCAGGA
	Rev: CCAGGTAGCTATGGTACTCCAGAA
<i>Npffr2</i>	Fw: CAGATTCCGCTGTGTGGTCT
	Rev: TCGCTCTCAGGGAATAGGCT
<i>Cd206</i>	Fw: GTTACCTGGAGTGATGGTTCTC
	Rev: AGGACATGCCAGGGTCACCTT
<i>Cd163</i>	Fw: GGCTAGACGAAGTCATCTGCAC
	Rev: CTTCGTTGGTCAGCCTCAGAGA
<i>Asic1</i>	Fw: CGACCTCCTGTGTACCCTTC
	Rev: CGTATGCTTGAGGGAGCAGT
<i>Npffr1</i>	Fw: AGAGTGATGCTGAAACCGCC
	Rev: CAGCTTCTCACGAAAGGGT
<i>Itgax (Cd11c)</i>	Fw: ACTGAGTGATGCCACTGTCTG
	Rev: TTGAGGCGAAGAGTGATCGG
<i>Fcgr1a (Cd64)</i>	Fw: TCCTCAATGCCAAGTGACCC
	Rev: CGCCATCGCTTCTAACTTGC

Human genes	Sequence
<i>BACTIN</i>	Fw: AGAGCTACGAGCTGCCTGAC
	Rev: AGCACTGTGTTGGCGTACAG
<i>NPFFR2</i>	Fw: GCCCCTTAGCGGGATATGAA
	Rev: TCCGGCTCCAGCTACTTTTC
<i>PPIA (CYPA)</i>	Fw: CTCGAATAAGTTTGACTTGTGTTT
	Rev: CTAGGCATGGGAGGGAACA
<i>MNDA</i>	Fw: TCGGAAGCAAGAGGGAGGAT
	Rev: CCACTGTCACTGGGTCGTTT
<i>CCL2 (MCP1)</i>	Fw: AGATGCAGTTAACGCCCCAC
	Rev: ACCCATTCCTTCTTGGGGTC
<i>RNF128</i>	Fw: TTCACGCTAAAGCCCCAGAG
	Rev: GACGCCCTCTCTCATAAGC
<i>AGMO</i>	Fw: CTGACCTGACTTCCATTGGATT
	Rev: CAAGCAACGGAGAGTTTCCATA
<i>IL4RA</i>	Fw: TTGCGAGTGGAAGATGAATG
	Rev: TTCACGCTAAAGCCCCAGAG

Supplemental Table 3. Metabolic parameters of human subjects of the study

Gender	Surgery date	Age	Dyslipidemia	Hypertension	Glucose metabolism	Height	Weight	BMI	Waist circumference	Glucose	HBA1C	Insulin	HOMA-IR	TRIGL	CHOL	LDLC	HDLC	NON-HDLC
1	17.06.2015	33/1	1	1	2	1.78	144.7	45.67	138,5	91	7.2	37.5	8.42	129	156	108	31	125
2	23.09.2015	58/8	1	1	3	1.56	114.3	46.97	127	93	5.9	5.2	1.19	93	175	128	36	139
1	10.06.2015	46/0	1	1	3	1.68	120.2	42.59	127	106	4.8	8.9	2.33	199	187	127	28	159
2	10.06.2015	51/3	1	2	3	1.64	118.2	43.95	118	108	5.7	10.2	2.72	114	169	104	52	117
1	08.07.2015	39/2	1	2	2	1,87	154	44.04	132	142	9.5	21.4	7.50	113	210	147	47	163
2	30.10.2015	61/7	2	1	2	1.61	100.8	38.89	115	93	5.6	24.7	5.67	108	187	135	38	149
2	28.10.2015	30/9	2	2	2	1.65	153.3	56.31	140	88	5	24.7	5.36	278	177	103	28	149
2	04.11.2015	57/7	1	1	3	1.5	98.4	43.73	127	101	5.8	13.8	3.44	74	166	106	55	111
1	04.11.2015	34/4	1	2	2	1.69	103.5	36.24	118	142	8.8	17.1	5.99	89	125	87	38	87
2	04.11.2015	51/7	1	2	2	1.49	125.8	56.66	143	125	8.7	31.7	9.77	205	287	212	35	252
2	11.11.2015	41/3	2	2	2	1.66	126.7	45.98	123	91	5.4	19.6	4.40	121	207	140	50	157
2	18.11.2015	43/0	2	1	3	1.58	96.4	38.62	106,5	85	5.5	10.7	2.24	94	168	117	41	127
2	16.12.2015	51/0	1	1	2	1.57	143.3	58.14	142	230	7.3	41.5	23.54	197	145	86	30	115
2	13.01.2016	23/9	2	2	3	1.7	138.6	47.96	117	82	5.1	20.3	4.11	80	114	67	43	71
2	13.01.2016	40/9	2	2	2	1.61	98.8	38.12	106	94	5.3	14.9	3.45	126	191	134	39	152
2	13.01.2016	59/4	2	1	2	1.5	92.4	41.07	122	103	5.8	23	5.84	105	153	98	44	109
1	13.01.2016	56/3	1	2	3	1.87	152	43.47	135	99	5.4	16.2	3.91	103	149.6	75	54	74.6
1	13.01.2016	45/2	2	2	2	1.65	143.2	52.53	141	102	5.2	18	4.53	102	148.4	69	59	79.4
1	NA	38/2	2	2	3	1.8	78	24.1	83	82.8	4	8.4	1.72	97	123	69	45	78
1	NA	62/1	2	1	3	1.76	77	24.9	81	93.6	3.9	6.3	1.46	67	121.4	65	47	74.4
1	NA	57/8	2	1	3	1.58	59	23.6	76	90	4.6	6	1.33	88	119	59	50	69

Supplemental Information

1	NA	24/6	2	2	3	1.9	82	22.7	86	88.2	5.1	7.6	1.66	90	123,8	65	49	74.8
1	NA	52/7	2	2	3	1.77	78	24.9	84	90	6.1	6.8	1.51	92	109,2	54	46	63.2
1	NA	51/0	2	2	3	1.65	61	22.4	77	91.8	4.9	8.5	1.93	98	119,8	67	44	75.8
1	NA	30/10	2	2	3	1.82	78	23.55	76	93.6	5.1	7.1	1.64	87	108,4	52	47	61.4
1	NA	41/5	2	2	3	1.8	78	24.07	85	95.4	5.8	5.1	1.20	78	113,6	56	48	65.6
1	NA	43/0	2	2	3	1.75	76	24.8	80	104.4	5.6	6.8	1.75	90	117,8	59	49	68.8
1	NA	23/9	2	2	3	1.78	72	22.7	81	93.6	5.5	4.9	1.13	75	118,6	61	48	70.6
1	NA	21/9	2	2	3	1.77	68	21.7	78	93.6	5.1	5.3	1.22	98	117	63	45	72
1	NA	37/0	2	2	3	1.79	76	23.7	81	97.2	4.5	6	1.44	91	124,4	68	47	77.4
1	NA	33/1	2	2	3	1.81	77	23.5	84	91.8	6.1	7.8	1.77	75	126,2	59	56	70.2
1	NA	26/0	2	2	3	1.72	70	23.6	84	99	5.3	6.5	1.59	87	113,8	61	44	69.8
1	NA	30/9	2	2	3	1.77	74	23.6	83	93.6	5.6	5.7	1.32	98	118,6	67	43	75.6
1	NA	45/1	2	2	3	1.73	68	22.7	76	97.2	4.1	6.1	1.46	99	123,6	66	48	75,6
2	NA	43/8	2	2	3	1.65	62	22.7	61	90	5	5.1	1.13	93	121,8	63	49	72.8
2	NA	34/10	2	2	3	1.68	65	23	63	84.6	5.5	7.9	1.65	87	120,4	58	52	68.4
2	NA	40/9	2	2	3	1.74	72	23.7	67	86.4	4.9	5.7	1.22	85	112,6	49	53	59.6
2	NA	36/0	2	2	3	1.78	72	22.7	76	88.2	4.4	7.2	1.57	72	118,2	57	51	67.2
2	NA	33/1	2	2	3	1.72	67	22.6	79	90	5.3	6.6	1.47	70	123,8	59	54	69.8
2	NA	58/8	2	2	3	1.73	70	23.3	65	91.8	5.4	7.3	1.65	82	126	60	55	71
2	NA	40/0	2	2	3	1.61	57	21.9	66	90	5.2	16.2	3.60	87	128,2	61	56	72.2
2	NA	50/3	2	2	3	1.58	55	22	63	93.6	5.1	8.1	1.87	67	127,4	65	52	75.4
2	NA	38/2	2	2	3	1.56	51	20.9	64	95.4	4.9	5.6	1.32	81	129,6	66	53	76.6
2	NA	60/8	2	2	3	1.59	54	21.3	68	90	5.6	7	1.56	85	126,6	63	53	73.6
2	NA	30/9	2	2	3	1.67	65	22.5	63	84.6	5.2	6.4	1.34	89	122,4	54	57	65.4

2	NA	27/10	2	2	3	1.64	63	23.4	61	88.2	4.7	5.3	1.15	82	135	69	55	80
2	NA	34/4	2	2	3	1.79	74	23.1	68	99	5.1	7	1.71	78	113.4	51	52	61.4
2	NA	51/7	2	2	3	1.64	63	23.4	63	91.8	5.6	6.4	1.45	72	117.6	54	53	64.6
2	NA	41/3	2	2	3	1.70	67	23.1	62	95.4	4.8	4.8	1.13	80	126.2	65	51	75.2
2	NA	23/0	2	2	3	1.76	72	23.2	64	91.8	5.4	5.5	1.25	78	127.8	63	54	73.8
1	NA	58	2	2	1	1.80	84	25.93		82.8	3.47	8.4	1.72	67	44	75.8	3.47	98
1	NA	48	2	2	1	1.87	100	28.6		93.6	6.6	6.3	1.46	86	59	54	69.8	16.6
2	NA	53	2	2	1	1.64	53	19.71		90	4.2	6	1.33	95	143	67	57	86
1	NA	38	2	2	1	1.79	74	23.1		88.2	4.3	7.6	1.66	78	144.6	53	76	68.6
2	NA	60	2	2	1	1.78	70	22.09		90	5.1	6.8	1.51	91	131.2	51	62	69.2
2	NA	51	2	2	1	1.53	78	33.32		91.8	5.3	8.5	1.93	83	136.6	59	61	75.6

Key:

Gender: 1 (male), 2 (female)

Age: years/months

Dyslipidemia: 1 (yes), 2 (no)

Hypertension: 1 (yes), 2 (no)

Glucose metabolism: type 1 diabetes (1), type 2 diabetes (2), normal (3)

Height: m

Weight: kg

Waist circumference: cm (when available)

Glucose: mg/dl

Insulin: mU/l

TRIGL: triglycerol, mg/dl

CHOL: total cholesterol, mg/dl

LDLC: low density lipoprotein cholesterol, mg/dl

HDLC: high density lipoprotein cholesterol, mg/dl

Study protocol was described before (12) .

Supplemental Methods

Mass spectrometry of plasma NPFF

Plasma protein concentration was determined by the Bradford assay. For analysis, we used samples adjusted to 10 µg/15 µl protein concentration (0.666 µg/µl) with 0.1% TFA. Mass spectrometry analysis was performed using the Orbitrap LC-MS platform (Thermo Scientific). The same approach was used control the purity of NPFF used in *in vitro* and *in vivo* assays.

Generation of NPFFR2 overexpressing transgenic mice

NPFFR2 overexpressing (NPFFR2-OE) mice were generated as described (13). C57BL/6 NPFFR2 cDNA was cloned into the pWHERE plasmid (InvivoGen, CA). NPFFR2-OE mice were generated on the C57BL/6 background (The Jackson Laboratory, Bar Harbor, ME) and maintained as heterozygotes (Ht). Littermate wild-type (WT) mice served as controls. Male mice (aged 8–12 weeks) were used in the study.

Generation of NPFFR2 knock-out (KO) mice

NPFFR2-KO mice were established by the Mouse Clinical Institute at the University of Strasbourg, using homologous recombination in mouse embryonic stem (ES) cells. The targeting vector contained LoxP sequences flanking exon 4 from NPFFR2 gene and FRT sequences flanking a neomycin resistance cassette. The targeting vector was introduced into ES cells by electroporation, and cells were selected for resistance to neomycin. Clones in which a homologous recombination took place were identified by PCR and confirmed by Southern blot. A positive clone was injected into a Balb/cN mouse blastocyst, which was implanted into a pseudo-pregnant female mouse, resulting in chimeric mice that were crossed with C57Bl/6N mice constitutively expressing Flip Recombinase to delete the resistance cassette. Resulting animals with floxed NPFFR2 exon 4 were then crossed with C57Bl/6N mice constitutively expressing Cre recombinase (CMV- Cre mice) to generate NPFFR2 knockout animals.

Genotyping of NPFFR2 knockout and WT mice used in this report was performed by PCR on genomic DNA from ear samples. Ear fragments were digested in 200 µL of lysis buffer (1 M Tris-HCl pH 8.5 20 ml, 0.5 MEDTA 2 ml, 10% SDS 4 ml, 5 M NaCl 8 ml, H₂O 166 ml) and 4 µl proteinase K (20 mg/mL Fermentas) overnight at 55°C in rotation in an oven. PCR reactions were performed using primers specific for wild-type (Lf: ACCCAGATTGAT-CGACAGGAATGAGA; Lr: CACCTAAAACCATCAGAAAATGCGTGT) and KO (Lf: AGGGACTTGCAGCATCTTGCTTTAAG; Er: GGGGACTAAGAGTTCTAAGGGG-CTGTC). PCR reactions (28 cycles: 1 × 94°C 3 min; 28 × (94°C 30 s; 68°C 30 s; 72°C 1 min); 1 × 4°C ∞) were performed in Buffer X (5 µl), NTPs (4 × 10 mM, 0.5µl), MgCl₂ (50 mM, 1.75 µl), Go Taq polymerase Promega (0.125 µl), H₂O (15.875 µl), 0.75 µl of each primer (10 mM) and genomic DNA (0.25 µl). DNA fragments amplified were then analyzed on an agarose gel (1.5%) after staining with ethidium bromide (0.5 µg/ml) and UV visualization. The size of the NPFFR2 KO and WT fragments are 369 and 353 bp, respectively.

The absence of NPFFR2 was confirmed by receptor binding assay. Briefly, cell membranes from olfactory bulbs were prepared as described before (14). The final pellet was resuspended in 12 volumes of cold 50 mM Tris-HCl buffer (pH 7.4), 0.32 M sucrose. Thirty micrograms of olfactory bulb membranes were incubated during 1 h at 25°C in a final volume of 300 µl in 50 mM Tris-HCl buffer (pH 7.4), 10 mM NaCl 0.1% BSA and 0.05 nM of [¹²⁵I]1DMeNPFF (binding buffer) in the absence or presence of 10 µM RFRP-3. Binding reactions were terminated by rapid filtration of the mixture on a Brandel filtration apparatus through GF/B Whatman filters preincubated in binding buffer. Filters were washed four times with ice-cold binding buffer. The amount of radioactivity retained on filters was determined by scintillation counting with a Tri-Carb 2100TR (Packard). Reactions were performed in duplicate.

Generation of Rnf128 conditional knock-out mouse

The Rnf128 conditional knock-out (Rnf128-KO) mouse was generated by the University of Wisconsin Biotechnology Center Transgenic Animal Facility. A recombineering strategy (15) was used to construct the Rnf128-KO targeting vector. The floxed exon 2 of Rnf128 leads to exon 2 deletion (bp 485–732) resulting in a premature stop codon at aa168 (bp 506). Briefly, a BAC clone containing the entire RNF128 gene was used as the source of genomic DNA from a 129/SvJ ES cell library (Invitrogen, Carlsbad CA). An 8 kb DNA fragment containing Rnf128 exon 2 and flanking sequences was introduced by recombineering into the vector pL253 vector to create the retrieval vector (G2-TK). A mini-targeting vector was constructed by PCR cloning of a loxP site, Rnf128 exon 2 along with 5' and 3' flanking sequences into pL451 that contained the FRT flanked PGK promoter/EM7 promoter-NEO-pGHpA cassette. The mini-targeting cassette was excised and transformed into recombination-competent DY380 cells transformed with G2-TK. Recombinants that integrated the pL451 cassette into G2-TK were selected with kanamycin. Restriction mapping and DNA sequencing was used to confirm the Rnf128-KO targeting vector. The Rnf128-KO targeting vector was linearized and introduced by electroporation into murine SV/129 R1 ES cells. ES cells that integrated the targeting vector either by

homologous or random integration were selected by growth on G418, replicated, and expanded. The targeted clones were identified by Southern blot, DNA sequence analysis, and karyotyping. The appropriately targeted ES cells were injected into C57BL/6 blastocysts to produce chimeric founders. After germline transmission of the targeted allele was confirmed in chimeras by PCR, chimeric mice on C57BL/6 × 129 background were crossed to FLPe-deleter mice and then backcrossed to C57BL/6 for 6 generations. Rnf128-KO mice were then crossed to Cre recombinase-expressing mice. Cre activity was screened for using genomic DNA from various tissues. cDNA was isolated from macrophages for Rnf128 RT-PCR.

Primer sequences used were as follows:

5' RNF128 exon 2: 5'-AGT CAC AAT GGT CAT CGA AG-3'

5' RNF128 genotyping: 5'-CAC ATG GTT AGA GCC CTT ATG GC-3'

3' RNF128 genotyping: 5'-GTT GGC TGT GTA CCC TTA GAG GT-3'

3' Neo: 5'-ATC CCC AGC ATG CCT GCT AT-3'

3' RNF128 RT-PCR: 5'-TAT CCA GAT GAT GCA GTC TC-3'

Assessment of glucose homeostasis in mice

Blood samples were collected from the lateral tail vein by venipuncture, and glucose levels were measured with a glucose tester (Hoffmann-La Roche or Bayer). NPDF, insulin and glucagon levels in plasma were assayed with commercial ELISA kits (Cloud-Clone Corp., Millipore; Crystal Chem, Zaandam, The Netherlands). Mass spectrometry of plasma NPDF and quality controls of the ELISA assay are provided in the Supplemental Figure 4. Sterile filtered glucose solution (1 g/kg bodyweight) was used to assay glucose tolerance of 4 h-fasted mice during the daytime. To estimate the level of gluconeogenesis, we i.p. injected mice with sodium pyruvate (1 g/kg) and blood glucose levels were determined prior to the administration and monitored over time. Insulin sensitivity was assayed by i.p. administration of insulin (1.5 IU/kg bodyweight, Novo Nordisk, Bagsvaerd, Denmark). Body temperature and food consumption was measured in metabolic cages (Tecniplast, Buguggiate, Italy).

AKT phosphorylation ELISA

Insulin-induced AKT phosphorylation was assayed as described (16). Liver, quadriceps muscle and fat depots were isolated 15 min after vehicle or insulin injection and frozen immediately in liquid nitrogen. Samples were homogenized in RIPA buffer with protease and phosphatase inhibitors and were used for ELISA assay as described in the manufacturers' protocols (AKT pS473 ELISA from AbCam, AKT pS308 from Cell Signaling Technology, Danvers, MA; total AKT ELISA from AbCam, Cambridge, UK).

Macrophage depletion *in vitro* and BrdU labeling of ATMs *in vivo*

To deplete ATMs, we used clodronate liposomes or empty liposomes (ClodLip BV, ClodronateLiposomes.org) as described (17, 18). For *in vitro* macrophage depletion, 50 µl of clodronate liposomes were added to 1 ml cell culture medium in six-well plates. To measure ATM proliferation, mice were i.p. injected with 100 mg/kg 5-bromo-2-deoxyuridine (BrdU, Sigma-Aldrich, St. Louis, MO) and BrdU incorporation was assessed by FACS analysis.

Histology and immunofluorescence staining

Tissue samples were fixed in 4% PFA diluted in PBS for 24 h and used for cryosectioning. Immunostainings were performed using antibodies listed in Supplemental Table 1. Positive controls (brain sections for NPDF) as well as negative controls lacking primary antibodies, as well as tissues proved negative for the desired antigens, were used. In order to avoid non-specific staining, we used poly-lysine pre-absorption and blocking with normal serum.

Analysis of plasma lipoproteins

Plasma samples were analyzed for cholesterol, triglycerol, HDL and LDL using commercial colorimetric assays (Sigma-Aldrich, St. Louis, MO).

Isolation of tissue resident macrophages and human PBMCs

Peritoneal lavage was used to collect peritoneal resident macrophages as described (19). Kupffer cells were isolated as described (20). Mouse primary bone marrow-derived macrophages (BMDMs) were obtained from the femur and maintained as described (19). PBMCs were collected from peripheral blood of healthy blood donors (n=4) as described (21). Phagocytosis activity of ATMs was measured as described before (19).

Cell culture of macrophage cell lines

All cell lines were purchased from ATCC. Mouse J774A.1 and RAW264.7 cells and human THP-1 cells were cultured in RPMI-1640 medium supplemented with 10% fetal bovine serum (FBS), 100 IU/ml penicillin and 100

µg/ml streptomycin, and were regularly checked for *Mycoplasma*. Culture medium of RAW264.7 cells was also supplemented with sodium pyruvate. For soft agar colony formation assays, we prepared 1% agarose in DMEM, which was added to 6-well plates. Cells were suspended in 0.5% agarose in DMEM and plated above the semi-solid 1% base agarose at 10,000 cells/well.

Overexpression of Ifi203 and Rnf128 in J774A.1 macrophages

J774A.1 macrophages were maintained in RPMI-1640 supplemented with 10% FBS, 100 IU/ml penicillin and 100 µg/ml streptomycin and were grown to 60% confluence in 6-well plates. Cells were transfected with 12 µg mouse Ifi203 or Rnf128 cDNA (OriGene, Rockville), using Attractane transfection reagent (Thermo Scientific, Waltham, MA), according to the manufacturer's instructions. Transfection efficiency was controlled by qPCR analysis of *Ifi203* mRNA and ELISA assay of Rnf128 protein.

NDRG2 overexpression in U937 macrophages

U937-mock and U937-NDRG2 cells were plated in a 24-well plate in RPMI 1640 medium containing 10% FBS. The cells were treated with 0.1 µg/ml PMA (Sigma-Aldrich, St. Louis, MO) for 2 days and then stimulated with 1 µg/ml LPS. Cells were harvested every 2 days, stained with 0.4% trypan blue, and live cells were counted using a hemocytometer. Proliferation was assessed by FACS analysis of Ki67 antigen expression.

Measurement of intracellular cAMP level

We used the cAMP-Glo™ Assay kit from Promega. The induction buffer was prepared by mixing serum-free RPMI 1640 medium with 100 mM Ro 20-1724 [4-(3-butoxy-4-methoxy-benzyl)imidazolidone] and 100 mM IBMX (3-isobutyl-1-methylxanthine), both previously diluted in DMSO. The cAMP-Glo™ Assay was performed with adherent macrophages using recommendations from Promega. Briefly, cells were grown in flasks and washed with PBS. After trypsinization, cells were collected and centrifuged at 1500 × *g* for 10 min. The resuspended cells were counted using the Nexcelom hemocytometer (Nexcelom Bioscience LLC.) or the Cellometer® Auto T4. Cells (10⁵ cells/ml) were plated in 96-well plates and incubated overnight in a cell culture incubator. On the next day, the medium was removed, and NPFF treatments were carried out in induction buffer. Luminescence intensity was measured with a Centro LB960 luminometer (Berthold Technologies, Bad Wildbad, Germany).

Receptor binding assay

FITC-conjugated NPFF was custom synthesized and purity was checked by HPLC. Serial dilutions of FITC-NPFF were added to 10⁶/ml macrophage suspensions. After 5 min, fluorescence intensity was measured using BD LSR II flow cytometer against untreated cells, counting 10,000 cells.

Transmission electron microscopy (TEM) of ATMs

Sorted NPFFR2⁺, Ki67⁺ or Ki67⁻ ATMs were collected in conical tubes, fixed in a 1:5 mixture of 1% glutaraldehyde and 4% PFA, and processed for embedding and ultrathin sectioning as described (19). The ultrathin sections were analyzed with a JEM Jeol 1010 transmission electron microscope.

Cell proliferation assay

For CCK8 assays, 10 µl of CCK-8 solution (Dojindo, Gaithersburg, MD) was added to each well of a 96-well plate every second day. After incubation for 2–3 h at 37°C, the absorbance at 450 nm was measured using a VICTOR3™ plate reader (PerkinElmer, Waltham, MA).

ELISA of IL-10, IL-6 and TNFα

Cell culture supernatants were assayed by IL-10 ELISA using a commercial kit (Mouse IL-10 Qantikine ELISA, R&D Systems, MN). Tissue lysates were assayed for IL-6 and TNFα using commercial kits (Thermo Fisher Scientific, Waltham and R&D Systems Minneapolis, MN) according to the manufacturers' protocol.

Nuclear translocation of NFκB

Cells were cultured on 6-well, glass-bottom culture plates designed for confocal microscopy (Ibidi, Planegg, Germany, ref. no. 543079). After treatment with LPS, NPFF, IL-10 neutralizing antibody (Abcam, Cambridge, UK), cells were fixed with 4% PFA for 30 min, washed with PBS and used for immunostaining against NFκB as described (22). After treatment with NPFF and LPS or IL-10 antibody, the cells were fixed with PFA and processed for immunostaining. Cells were permeabilized with 0.1% Triton X diluted in PBS and stained overnight with polyclonal rabbit antibody against mouse NFκB (Cell Signaling Technology, Danvers, MA).

Detection of neutral lipids in tissue sections

Liver specimens were fixed in 4% PFA diluted in PBS, and fixed overnight. Sections were cut with a Leica vibratome, and stained with 0.5% Oil red-O (Sigma-Aldrich, St. Louis, MO) in n-propanol for 20 min, cleared with n-propanol and covered for microscopy with Aquatex mounting medium (Merck, Millipore, Billerica, MA).

Western blotting

Cells were lysed in ice-cold RIPA buffer supplemented with protease and phosphatase inhibitors (Complete ULTRA; PhosphoStop, Roche, Basel, Switzerland) and treated with DNase (Sigma-Aldrich, St. Louis). Protein lysates were processed and 40 µg protein samples were run on 10% SDS gels for western blotting. Antibodies used are listed in Supplemental Table 1. For pSTAT-6 western blotting, cells were serum starved for 4 h prior treatments, and IL-4 was used at 100 ng/ml concentration.

ELISA of pSTAT-6, STAT-6, pSTAT-3 and STAT-3

To assess STAT phosphorylation, we used in-cell ELISA kits, according to the manufacturers' protocols. Briefly, macrophages were cultured in 96-well plates, and after treatment the cells were fixed and processed for ELISA. For detection of total STAT-6 and tyrosine-phosphorylated pSTAT-6 we used the in-cell ELISA kit from Thermo Fisher Scientific (Waltham, MA). The level of pSTAT-6 was normalized to total STAT-6 and cellular protein content, measured by Janus green staining. For STAT-3 and pSTAT-3 measurement we used the in-cell ELISA kit from Sigma-Aldrich.

ELISA of mouse E3 ubiquitin ligase Rnf128

Cells were lysed in ice-cold RIPA buffer supplemented with protease inhibitors (Complete ULTRA, Roche, Basel, Switzerland), and assayed by ELISA (MyBioSource, MBS9326485) according to the manufacturer's instructions. Rnf128 levels were normalized to protein content of the lysates.

Affymetrix gene expression analysis

Samples with sufficient quantity and quality of RNA were subjected to gene expression analysis using Affymetrix expression arrays, and scaled normalized gene expression values were produced as described (23). Briefly, GeneChip Mouse or Human Gene 2.0 Arrays were used. RNA samples (500 ng) were processed and labeled for array hybridization using the Ambion WT Expression kit (Life Technologies, 4411974). Labeled, fragmented cDNA (Affymetrix GeneChip® WT Terminal Labeling and Controls Kit, 901524) was hybridized to the arrays for 16 h at 45°C (at 60 rpm) (Affymetrix GeneChip® Hybridization, Wash, and Stain Kit, 900720). Arrays were washed and stained using the Affymetrix Fluidics Station 450 and scanned using the Hewlett-Packard GeneArray Scanner 3000 7G.

Laser-capture and gene expression profiling of human islets

Frozen tissue (OCT) sections were obtained from the nPOD tissue collection (24). Tissue slides were fixed, and laser-capture of islets was conducted as described (25). All islets in 2–5 sections of tissue from each donor were captured, pooled and RNA extracted using the Arcturus PicoPure RNA Isolation Kit (Applied Biosystems, NY). Quality and quantity of RNA was determined on a Bioanalyzer 2100 instrument (Agilent Technologies, CA). Samples with sufficient quantity and quality of RNA were then subjected to gene expression analysis using Affymetrix expression arrays, and scaled normalized gene expression values produced as previously described (23).

Supplemental References

1. Ampem G, Azegrouz H, Bacsadi A, Balogh L, Schmidt S, Thuroczy J, and Roszer T. Adipose tissue macrophages in non-rodent mammals: a comparative study. *Cell and tissue research*. 2016;363(2):461-78.
2. Cittaro D, Lampis V, Luchetti A, Coccurello R, Guffanti A, Felsani A, Moles A, Stupka E, FR DA, and Battaglia M. Histone Modifications in a Mouse Model of Early Adversities and Panic Disorder: Role for *Asic1* and Neurodevelopmental Genes. *Scientific reports*. 2016;6(25131).
3. Ayachi S, and Simonin F. Involvement of Mammalian RF-Amide Peptides and Their Receptors in the Modulation of Nociception in Rodents. *Frontiers in endocrinology*. 2014;5(158).
4. Quillet R, Ayachi S, Bihel F, Elhabazi K, Ilien B, and Simonin F. RF-amide neuropeptides and their receptors in Mammals: Pharmacological properties, drug development and main physiological functions. *Pharmacology & therapeutics*. 2016;160(84-132).

5. Chera S, Baronnier D, Ghila L, Cigliola V, Jensen JN, Gu G, Furuyama K, Thorel F, Gribble FM, Reimann F, et al. Diabetes recovery by age-dependent conversion of pancreatic delta-cells into insulin producers. *Nature*. 2014;514(7523):503-7.
6. Nickelson KJ, Stromsdorfer KL, Pickering RT, Liu TW, Ortinau LC, Keating AF, and Perfield JW, 2nd. A comparison of inflammatory and oxidative stress markers in adipose tissue from weight-matched obese male and female mice. *Experimental diabetes research*. 2012;2012(859395).
7. Bigornia SJ, Farb MG, Mott MM, Hess DT, Carmine B, Fiscale A, Joseph L, Apovian CM, and Gokce N. Relation of depot-specific adipose inflammation to insulin resistance in human obesity. *Nutrition & diabetes*. 2012;2(e30).
8. Patsouris D, Li PP, Thapar D, Chapman J, Olefsky JM, and Neels JG. Ablation of CD11c-positive cells normalizes insulin sensitivity in obese insulin resistant animals. *Cell metabolism*. 2008;8(4):301-9.
9. Fujisaka S, Usui I, Bukhari A, Iikutani M, Oya T, Kanatani Y, Tsuneyama K, Nagai Y, Takatsu K, Urakaze M, et al. Regulatory mechanisms for adipose tissue M1 and M2 macrophages in diet-induced obese mice. *Diabetes*. 2009;58(11):2574-82.
10. Zhuang G, Meng C, Guo X, Cheruku PS, Shi L, Xu H, Li H, Wang G, Evans AR, Safe S, et al. A novel regulator of macrophage activation: miR-223 in obesity-associated adipose tissue inflammation. *Circulation*. 2012;125(23):2892-903.
11. Rusinova I, Forster S, Yu S, Kannan A, Masse M, Cumming H, Chapman R, and Hertzog PJ. Interferome v2.0: an updated database of annotated interferon-regulated genes. *Nucleic acids research*. 2013;41(Database issue):D1040-6.
12. Gayoso-Diz P, Otero-Gonzalez A, Rodriguez-Alvarez MX, Gude F, Garcia F, De Francisco A, and Quintela AG. Insulin resistance (HOMA-IR) cut-off values and the metabolic syndrome in a general adult population: effect of gender and age: EPIRCE cross-sectional study. *BMC endocrine disorders*. 2013;13(47).
13. Lin YT, Kao SC, Day YJ, Chang CC, and Chen JC. Altered nociception and morphine tolerance in neuropeptide FF receptor type 2 over-expressing mice. *European journal of pain*. 2016;20(6):895-906.
14. Gherardi N, and Zajac JM. Neuropeptide FF receptors of mouse olfactory bulb: binding properties and stimulation of adenylate cyclase activity. *Peptides*. 1997;18(4):577-83.
15. Liu P, Jenkins NA, and Copeland NG. A highly efficient recombineering-based method for generating conditional knockout mutations. *Genome research*. 2003;13(3):476-84.
16. Sabio G, Das M, Mora A, Zhang Z, Jun JY, Ko HJ, Barrett T, Kim JK, and Davis RJ. A stress signaling pathway in adipose tissue regulates hepatic insulin resistance. *Science*. 2008;322(5907):1539-43.
17. Bu L, Gao M, Qu S, and Liu D. Intraperitoneal injection of clodronate liposomes eliminates visceral adipose macrophages and blocks high-fat diet-induced weight gain and development of insulin resistance. *The AAPS journal*. 2013;15(4):1001-11.
18. Feng B, Jiao P, Nie Y, Kim T, Jun D, van Rooijen N, Yang Z, and Xu H. Clodronate liposomes improve metabolic profile and reduce visceral adipose macrophage content in diet-induced obese mice. *PloS one*. 2011;6(9):e24358.
19. Röszer T, Menendez-Gutierrez MP, Lefterova MI, Alameda D, Nunez V, Lazar MA, Fischer T, and Ricote M. Autoimmune kidney disease and impaired engulfment of apoptotic cells in mice with macrophage peroxisome proliferator-activated receptor gamma or retinoid X receptor alpha deficiency. *Journal of immunology*. 2011;186(1):621-31.
20. Li PZ, Li JZ, Li M, Gong JP, and He K. An efficient method to isolate and culture mouse Kupffer cells. *Immunology letters*. 2014;158(1-2):52-6.
21. Davies JQ, and Gordon S. Isolation and culture of human macrophages. *Methods in molecular biology*. 2005;290(105-16).
22. Trask OJ, Jr. In: Sittampalam GS, Coussens NP, Nelson H, Arkin M, Auld D, Austin C, Bejcek B, Glicksman M, Inglese J, Iversen PW, et al. eds. *Assay Guidance Manual*. Bethesda (MD); 2004.

23. Wu J, Kakoola DN, Lenchik NI, Desiderio DM, Marshall DR, and Gerling IC. Molecular phenotyping of immune cells from young NOD mice reveals abnormal metabolic pathways in the early induction phase of autoimmune diabetes. *PLoS one*. 2012;7(10):e46941.
24. Campbell-Thompson M, Wasserfall C, Kaddis J, Albanese-O'Neill A, Staeva T, Nierras C, Moraski J, Rowe P, Gianani R, Eisenbarth G, et al. Network for Pancreatic Organ Donors with Diabetes (nPOD): developing a tissue biobank for type 1 diabetes. *Diabetes/metabolism research and reviews*. 2012;28(7):608-17.
25. Richardson SJ, Rodriguez-Calvo T, Gerling IC, Mathews CE, Kaddis JS, Russell MA, Zeissler M, Leete P, Krogvold L, Dahl-Jorgensen K, et al. Islet cell hyperexpression of HLA class I antigens: a defining feature in type 1 diabetes. *Diabetologia*. 2016.